Cellular/Molecular

Brain Tumor Regulates Neuromuscular Synapse Growth and Endocytosis in *Drosophila* by Suppressing Mad Expression

Wenwen Shi,[1]* **Yan Chen,**[1]* **Guangming Gan,**[2] **Dan Wang,**[1] **Jinqi Ren,**[1] **Qifu Wang,**[1] **Zhiheng Xu,**[1] **Wei Xie,**[2] **and Yong Q. Zhang**[1]

[1]Key Laboratory of Molecular and Developmental Biology, Institute of Genetics and Developmental Biology, Chinese Academy of Sciences, Beijing 100101, China, and [2]Key Laboratory for Developmental Genes and Human Disease, Ministry of Education, Institute of Life Sciences, Southeast University, Nanjing 210096, China

The precise regulation of synaptic growth is critical for the proper formation and plasticity of functional neural circuits. Identification and characterization of factors that regulate synaptic growth and function have been under intensive investigation. Here we report that brain tumor (brat), which was identified as a translational repressor in multiple biological processes, plays a crucial role at *Drosophila* neuromuscular junction (NMJ) synapses. Immunohistochemical analysis demonstrated that *brat* mutants exhibited synaptic overgrowth characterized by excess satellite boutons at NMJ terminals, whereas electron microscopy revealed increased synaptic vesicle size but reduced density at active zones compared with wild-types. Spontaneous miniature excitatory junctional potential amplitudes were larger and evoked quantal content was lower at *brat* mutant NMJs. In agreement with the morphological and physiological phenotypes, loss of Brat resulted in reduced FM1-43 uptake at the NMJ terminals, indicating that *brat* regulates synaptic endocytosis. Genetic analysis revealed that the actions of Brat at synapses are mediated through mothers against decapentaplegic (Mad), the signal transduction effector of the bone morphogenetic protein (BMP) signaling pathway. Furthermore, biochemical analyses showed upregulated levels of Mad protein but normal mRNA levels in the larval brains of *brat* mutants, suggesting that Brat suppresses Mad translation. Consistently, knockdown of *brat* by RNA interference in *Drosophila* S2 cells also increased Mad protein level. These results together reveal an important and previously unidentified role for Brat in synaptic development and endocytosis mediated by suppression of BMP signaling.

Introduction

The synapse is a specialized intercellular junction devoted to communication between neurons and their targets. Proper growth and regulation of synapses are critical to the normal neuronal function. The *Drosophila* neuromuscular junction (NMJ) is an effective model system to dissect molecular mechanisms of synaptic development. Multifarious factors and molecular signaling pathways, such as actin regulators, endocytic proteins,

ubiquitin-mediated protein degradation, bone morphogenetic protein (BMP), and wingless (Wnt) pathways play important roles at *Drosophila* NMJ synapses (Collins and DiAntonio, 2007; O'Connor-Giles et al., 2008; Giagtzoglou et al., 2009; Ball et al., 2010; Bayat et al., 2011).

BMP signaling is a major retrograde growth-promoting pathway at *Drosophila* NMJ synapses (Collins and DiAntonio, 2007; O'Connor-Giles et al., 2008; Ball et al., 2010; Bayat et al., 2011). The retrograde BMP signaling cascade is initiated by release of the ligand Glass bottom boat (Gbb) from the postsynaptic muscle and subsequent binding to the presynaptic type II BMP receptor wishful thinking (Wit). Upon ligand binding, Wit forms a complex with the type I receptors thickvein (Tkv) and saxophone (Sax), resulting in their phosphorylation. In turn, phosphorylated type I receptors phosphorylate the Smad family transcriptional factor mothers against decapentaplegic (Mad). Mad is a signal transduction effector that, when phosphorylated, translocates to the nucleus of motoneurons to regulate transcription of target genes that control NMJ growth (Collins and DiAntonio, 2007; Ball et al., 2010; Bayat et al., 2011).

Brain tumor (Brat) contains multiple protein-protein interaction domains and is conserved throughout evolution from *Caenorhabditis elegans* to humans (Arama et al., 2000). Brat acts as a translational repressor in multiple developmental contexts through distinct mechanisms. During early embryogenesis, Brat forms a complex with the RNA-binding proteins Pumilio (Pum) and Nanos (Nos) and the RNA 5′ cap-binding protein d4EHP

(the *Drosophila* homolog of eIF4E) to suppress the translation of the morphogen Hunchback in the posterior (Sonoda and Wharton, 2001; Edwards et al., 2003; Cho et al., 2006). In the female germline, Brat acts together with Pum to repress the expression of Mad and the growth regulator dMyc to promote germline differentiation (Harris et al., 2011). During larval neurogenesis, Brat controls neuroblast self-renewal and neuronal differentiation (Bello et al., 2006; Betschinger et al., 2006; Lee et al., 2006; Stefanatos and Vidal, 2011). In the postmitotic neurons, Brat interacts with Pum and Nos to translationally repress the voltage-gated sodium channel subunit *paralytic* (*para*) and thereby modulate the excitability of motor neurons (Muraro et al., 2008). Pum and Nos regulate NMJ synapse development (Menon et al., 2004, 2009), but a possible role for Brat at synapses has not been demonstrated.

We report here that the NMJ terminals of *brat* mutants exhibit more numerous satellite boutons than do wild-type and that these mutant NMJs have reduced neurotransmission efficiency and defective endocytosis. Furthermore, our data indicate that Brat regulates synapse development and endocytosis by suppressing translation of the BMP signaling component Mad. Thus, our study unravels a novel role for *brat* at the NMJ and offers new insight into the regulation of BMP signaling for NMJ growth.

Materials and Methods

Drosophila stocks and genetics. Flies of either sex were cultured in standard cornmeal media at 25°C unless otherwise indicated. The *w[1118]* strain was used as the wild-type control. Other fly strains used were motor neuron-specific *Ok6-Gal4* from M. O'Connor (University of Minnesota, Saint Paul, MN) and muscle-specific *Mhc-Gal4* from C. Goodman (Howard Hughes Medical Institute, Chevy Chase, MD). The mutant *brat[11]* strain was from D. Frank (Washington University, St. Louis, MO; Frank et al., 2002), both *brat[150]* and *brat[192]* were from J. Knoblich (Institute of Molecular Biotechnology, Vienna, Austria; Betschinger et al., 2006), *UAS-brat[RNAi]* was from the Vienna *Drosophila* RNAi Center (No. V31333), and *UAS-brat* was from R. Wharton (The Ohio State University, Columbus, OH; Sonoda and Wharton, 2001). The Mad mutant *mad[12]* was from S. J. Newfeld (Arizona State University, Tempe, AZ; Takaesu et al., 2005). A *mad* RNAi transgenic line was from E. M. De Robertis (Howard Hughes Medical Institute, Los Angeles, CA; Eivers et al., 2009). The remaining strains, *da-Gal4, elav-Gal4, wit[A12], tkv[7], dad[J1E4]*, and *Df(2L)BSC162*, were obtained from the Bloomington Stock Center. For rescue experiments, meiotic recombination (*OK6-Gal4, brat[11]/CyO-GFP*) and interchromosomal combinations (*elav-Gal4; brat[11]/CyO-GFP, brat[11]/CyO-GFP; Mhc-Gal4/TM6B*, and *brat[192]/CyO-GFP; UAS-flag-brat/TM6B*) were constructed according to conventional procedures. For *elav-Gal4* rescue, only female progeny were collected for analyses. The identities of the recombinants as parental stocks were verified by phenotypic and immunochemical analyses. Nonbalancer progeny were selected to examine rescue effects.

Immunohistochemical analyses. Dissections and immunohistochemical analyses of wandering third-instar larvae of either sex were performed as described previously (Jin et al., 2009; Yao et al., 2011). For immunostaining of Brp and glutamate receptors, larvae were dissected in a normal medium (128 mM NaCl, 2 mM KCl, 4 mM MgCl$_2$, 35.5 mM sucrose, and 5 mM HEPES, pH 7.3; Jan and Jan, 1976) supplemented with 2 mM L-glutamate and fixed in ice-cold methanol for 5 min. For immunostaining of other proteins, late third-instar larvae were dissected in Ca^{2+}-free standard saline and fixed in 4% paraformaldehyde for 30–60 min. The following monoclonal antibodies were obtained from the Developmental Studies Hybridoma Bank: anti-CSP(cysteine-string protein; 6D6; 1:500), anti-Bruchpilot (nc82; 1:50), anti-GluRIIA (1:50), and anti-Discs large (Dlg; 4F3; 1:1000). Other antibodies used included rabbit anti-phosphorylated Mad (1:500) from P. ten Dijke (Leiden University, Leiden, the Netherlands; Persson et al., 1998), rabbit anti-glutamate receptor IID (GluRIID; 1:2500) from S. Sigrist (Free University Berlin, Berlin, Germany; Qin et al., 2005), rabbit GluRIIB from (1:2500) from A.

DiAntonio (Washington University, WA), anti-Flag (Sigma-Aldrich No. F3165; 1:2000), and FITC- and Texas red-conjugated anti-horseradish peroxidase (HRP; 1:200) from Jackson ImmunoResearch. The corresponding secondary antibodies, goat anti-mouse and goat anti-rabbit IgGs labeled with Alexa Fluor 488 or 568 (Invitrogen), were used at 1:1000. Motor neuron nuclei were labeled with TO-PRO-3 iodide (Invitrogen No. T3605; 1:2000). All images were acquired with a Leica SP5 confocal microscope and processed using Adobe Photoshop 8.0.

For quantification of bouton number, images of NMJ 4 stained with anti-CSP were analyzed with NIH ImageJ as described previously (Jin et al., 2009; Yao et al., 2011). Satellite boutons were defined as the small boutons emanating from the NMJ branch or from larger parental boutons (Dickman et al., 2006; O'Connor-Giles et al., 2008). For quantification of pMad level at NMJs, staining intensities were measured within the HRP-positive NMJ 4 in abdominal segments A2 and A3. For quantification of pMad level in motor neuron nuclei, staining intensities normalized to the nuclei dye signals were quantified with ImageJ software.

Western analysis and S2 cell culture. Western blotting analysis of larval brains and Schneider 2 (S2) cells were conducted as previously described (Jin et al., 2009; Wang et al., 2010) using the following primary antibodies: anti-Flag (Sigma No. F3165; 1:20000), anti-pMad (Cell Signaling Technology No. 9516; 1:1000), anti-Mad (Santa Cruz Biotechnology No. 15810; 1:500), and anti-actin (Millipore Bioscience Research Reagents No. mAb1501; 1:100,000). The secondary HRP-labeled antibodies were obtained from Sigma-Aldrich. Protein bands were visualized with an ECL kit from Millipore. S2 cells were cultured in Sf-900 II serum-free medium (Invitrogen No. 10902). A *brat* dsRNA, produced according to Harris et al. (2011), was transfected using Cellfectin II (Invitrogen No. 10362) according to the manufacturer's instructions. Cells were harvested for Western analysis 2 d after transfection.

Transgenic constructs and anti-brat antibodies. A UAS-Flag-Brat construct was generated using the *Drosophila* Gateway Vector system. The Brat coding sequence was amplified from a cDNA clone (DGRC LD16270) by PCR and recombined into the pCR8/GW/TOPO vector (Invitrogen No. k250020). After the *in vitro* recombination reaction between the entry clone and a destination vector (DGRC, pTFMW), the *UAS-flag-brat* expression clone was generated. Brat polyclonal antibodies were raised in rats against a His-tagged fusion protein bearing amino acid residues 723–1037 of Brat. For immunostaining, the antibody was used at a 1:400 dilution. Brat monoclonal antibody 3A9 was generated in mouse using a His fusion protein bearing Brat amino acid residues 367–767 and a GST fusion protein bearing Brat amino acid residues 723–1037 at a ratio of 1:1. The 3A9 antibody recognized both peptides of 367–767 and 723–1037 aa as indicated by an ELISA assay. For Western analysis, 3A9 was used at a 1:1000 dilution.

Quantification of Mad mRNA level. Total RNA was isolated from third-instar larval brains of the various genotypes using Trizol Reagent (Invitrogen No. 15596) according to the manufacturer's instructions. Total RNA was reverse transcribed into single-stranded cDNA using SuperScript III First-Strand Synthesis System (Invitrogen No. 18080). Quantitative PCR was performed using the Agilent Mx3000p real-time PCR detection system and the QuantiTect SYBR Green PCR kit (Qiagen No. 204141). The primers for detecting *mad* mRNA were as follows: 5′-AATCCGTGGTGGTAGTTGCAG-3′ and 5′-AACAACTCCGTGATCGTTGAC-3′. The primers 5′-GCTGAGCGTGAAATCGTCCGTG-3′ and 5′-CCCAAGAACGAGGGCTGGAACA-3′ were used to detect *actin* mRNA. The expression level of *mad* mRNA was normalized to that of actin mRNA. At least three biological repeats were performed for statistical analysis.

FM1-43 uptake assay. For the FM1-43 dye loading assay, we followed previously published protocols (Verstreken et al., 2008; Wang et al., 2010). Late third-instar larvae were dissected in the normal medium (128 mM NaCl, 2 mM KCl, 4 mM MgCl$_2$, 35.5 mM sucrose, and 5 mM HEPES, pH 7.3; Jan and Jan, 1976), then washed with 1.5 mM Ca^{2+} normal medium for 30 s. Motor axons innervating muscles were gently cut without disturbing the underlying musculature to eliminate electrical firing from the CNS. To load the fluorescent FM1-43 dye (Invitrogen No. T-35356) into boutons, preparations were incubated for 5 min in high-K$^+$ (90 mM) saline containing 10 μM FM1-43 (Invitrogen), and then vigorously washed three times for 5 min per wash in Ca^{2+}-free saline. For the rescue experiments, flies were cultured at 18°C

starting from the embryo stage and the FM1-43 uptake assay was also performed at 18°C. The loaded synapses were imaged on a Leica SP5 confocal microscope using a 40× water-immersion lens.

Electron microscopy and morphometric analysis. Larval tissue sections for EM analysis were prepared according to procedures described previously (Liu et al., 2010; Liu et al., 2011). Wandering third-instar larvae were dissected in HL-3 saline (128 mM NaCl, 2 mM KCl, 4 mM MgCl$_2$, 35 mM sucrose, 5 mM HEPES, pH 7.4) and fixed at 4°C overnight in a mixture of 2% glutaraldehyde and 2% formaldehyde in 0.1 M sodium cacodylate buffer, pH 7.4, followed by several rinses with cacodylate buffer. Right and left hemi-segments from abdominal segment A2 or A3 were separated from the larval fillets and postfixed for 2 h with 1% OsO$_4$ in cacodylate buffer. The preparations were stained *en bloc* for 1 h with saturated uranyl acetate in 50% ethanol before dehydration in a graded series of ethanol solutions. The samples were embedded in Spurr resin (Sigma-Aldrich). Serial longitudinal ultrathin sections (70 nm thick) of NMJ 6/7 were prepared on a Leica UC6 ultramicrotome using a diamond knife. Grids were poststained with saturated uranyl acetate in 50% ethanol and 1% lead citrate (pH 12) and examined under a Jeol JEM-1230 electron microscope. Images of sections through the midline of type 1b boutons were captured with a Ganton820 digital CCD camera. For quantification of the size and density of synaptic vesicles (SVs) at active zones, images of >20 individual boutons from at least four animals of each genotype were analyzed. The diameters and the number of SVs within a 200 nm radius of the transmitter release site (T-bar) were measured using ImageJ.

Electrophysiology. Excitatory junctional potentials (EJPs) and spontaneous miniature EJPs (mEJPs) at NMJs were recorded using intracellular electrodes (Jin et al., 2009; Wang et al., 2010). Wandering third-instar larvae were dissected in Ca^{2+}-free HL3.1 saline. The gut and fat were removed and the body wall was spread open to expose the nerves and muscles. Intracellular microelectrodes were pulled from borosilicate glass (World Precision Instruments) on a glass puller (P-2000, Sutter Instrument) and filled with 3 M KCl. Electrodes with resistances of 10–20 MΩ were used for the experiments. Recordings were performed at 18°C with an Axoclamp 2B amplifier (Molecular Devices) in Bridge mode. Data were digitized with a Digidata 1322A digitizer (Molecular Devices) and acquisition was controlled by Pclamp 9.1 (Molecular Devices). Both EJP and mEJPs were recorded in HL3.1 saline containing 0.23 mM Ca^{2+}. For EJP recordings, a Grass S48 stimulator with SIU-5 isolator (Astro-Grass) coupled to a suction electrode was used to stimulate the nerve with 0.3 Hz suprathreshold pulses. A total of 25–30 EJPs were recorded from NMJ 6 of abdominal segment A3 for each animal, followed by mEJP recording for 120 s. Only recordings from muscles with resting membrane potentials more polarized than 50 mV and input resistances >6 MΩ were analyzed. All data were
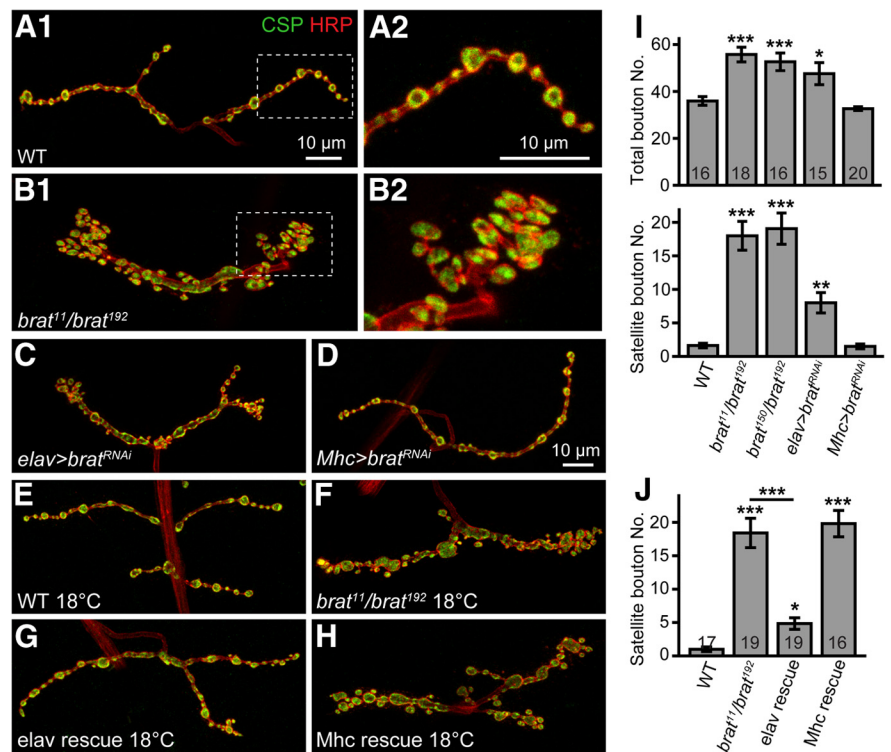

Figure 1. *brat* mutants have more numerous satellite boutons. All images are projections of confocal z-stacks of NMJ 4 synapses from abdominal segment A2 or A3 of a third-instar larva double-labeled with anti-CSP (green) and anti-HRP (red). *A–D*, *brat* mutants and flies with presynaptic but not postsynaptic RNAi knockdown of *brat* showed excess satellite boutons instead of the typical boutons arranged in a "beads-on-a-chain" pattern in wild-type. *A2*, *B2*, Boxed areas in *A1* and *B1*, respectively, at higher magnification. The genotypes are wild-type (*A*), *brat¹¹/brat¹⁹²* (*B*), elav-Gal4/UAS-brat^RNAi^ (*C*), and UAS-brat^RNAi^/+; Mhc-Gal4/+ (*D*). *E–H*, The increased number of satellite boutons in *brat* mutants was rescued by presynaptic but not postsynaptic expression of *brat* at 18°C. The genotypes are wild-type (*E*), *brat¹¹/brat¹⁹²* (*F*), and presynaptic (*G*) and postsynaptic (*H*) expression of *brat* on a *brat* mutant background (*G*, elav-Gal4; *brat¹¹/brat¹⁹²*; UAS-flag-brat/+ and *H*, *brat¹¹/brat¹⁹²*; Mhc-Gal4/UAS-flag-brat). Scale bar, 10 μm. *I*, *J*, Bar graphs showing statistical results of total and satellite bouton number at 25°C (*I*) and satellite bouton number at 18°C (*J*) of different genotypes. The number of animals analyzed for each genotype is indicated in the column. Statistical significance was calculated using one-way ANOVA (*$p < 0.05$; **$p < 0.01$; ***$p < 0.001$; error bars denote SEM).

Figure 2. Characterization of loss- and gain-of-function mutants of *brat* by immunochemical analysis. *A*, *B*, The ventral nerve cord (VNC) of third-instar larvae of wild-type (*A*) and *brat¹¹/brat¹⁹²* mutants (*B*) was stained with a rat anti-Brat serum. *C*, Anti-Flag staining of VNC-expressing Flag-Brat pan-neuronally under the control of elav-Gal4 (elav-Gal4/+; UAS-flag-brat/+). *D1–D3*, Enriched expression of Flag-Brat in the soma of motoneurons in the VNC costained with anti-Flag (*D1*, green) and anti-Brat (*D2*, red). Flag-Brat was overexpressed in motor neurons driven by OK6-Gal4 in *brat* mutant background (OK6-Gal4/+, brat¹¹/brat¹⁹²; UAS-flag-brat/+). *E*, Western analysis of larval brains with a monoclonal anti-Brat antibody 3A9. The genotypes are as follows: wild-type, *brat¹¹/brat¹⁹²*, *brat¹⁵⁰/brat¹⁹²*, UAS-brat^RNAi^/+; da-Gal4/+, and elav-gal4/+; UAS-brat/+. *F*, Identification of UAS-flag-brat transgenic lines (elav-Gal4/+; UAS-flag-brat/+) by Western blotting using anti-Flag and the monoclonal anti-Brat 3A9.

Figure 3. *brat* mutant boutons have fewer but larger SVs at active zones. Micrographs of synaptic boutons from wild-type (***A,C,E***) and *brat[11]*/*brat[192]* mutants (***B,D,F***) are shown. Mitochondria (M), AZs, and SSR are indicated in ***A*** and ***B***. ***C–F*** show active zones with SVs clustered around a T-bar at higher magnification. Arrowheads in ***C*** and ***D*** indicate electron-dense membranes; arrows in ***D*** denote presynaptic membrane ruffles. Arrowheads in ***F*** indicate enlarged vesicles around T-bar. Scale bars: ***B***, 500 nm; ***D***, 200 nm; and ***F***, 100 nm. ***G***, Bar graphs showing statistical results of mean vesicle number per square micrometer of cross-sectioned boutons. ***H, I***, Bar graphs showing statistical results of mean PSD length (***H***) and the number of presynaptic membrane ruffles per AZ (***I***). ***J, K***, Bar graphs showing statistical analyses of the number and diameter of SVs within a 200 nm radius of active zones demarcated by dashed lines in ***E*** and ***F***. ***L, M***, The frequency distribution and cumulative probability plot of vesicle diameters in the defined area of AZs ($n = 676$ for wild-type and $n = 735$ for mutants from ≥ 4 animals). Statistical significance was calculated using Student's *t* test (*$p < 0.05$; ***$p < 0.001$; error bars denote SEM).
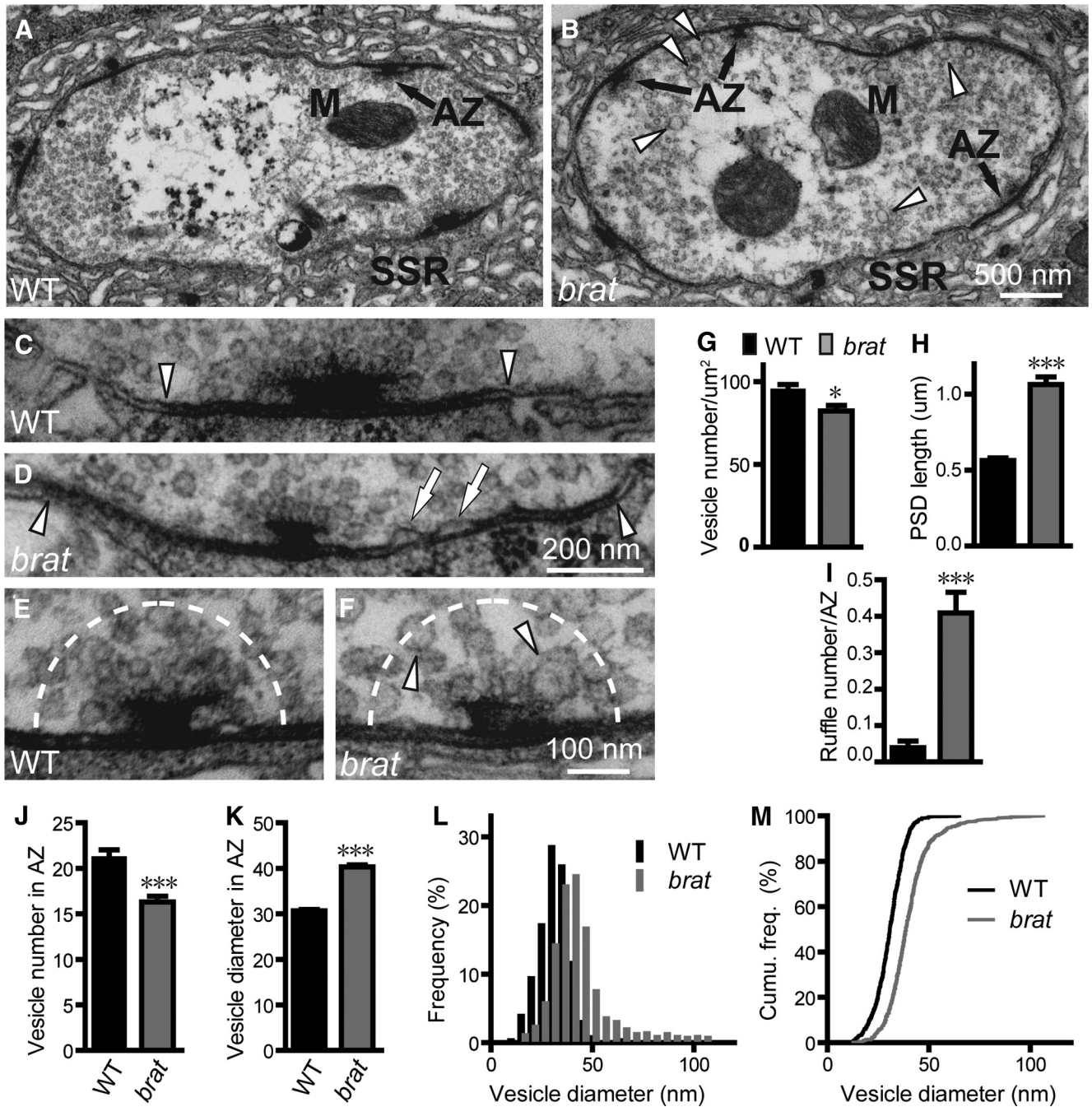
analyzed with Clampfit 9.1 software. Quantal content was calculated by dividing the mean EJP amplitude corrected for nonlinear summation by the mean mEJP amplitude with a reversal potential of 0 mV according to Martin's equation (Martin, 1955).

Statistical analyses. All data are expressed as mean $\pm$ SEM. Statistical comparisons were performed using SPSS 18.0. For multiple comparisons among the different genotypes in Figures 1 and 5–9, one-way ANOVAs with *post hoc* multiple pairwise comparisons were performed. For pairwise comparisons between wild-type *Drosophila* and mutants in Figures

3 and 4, two-tailed Student's *t* tests were performed (*$p < 0.05$, **$p < 0.01$, and ***$p < 0.001$; error bars indicate SEM).

Results

brat regulates synaptic growth

To characterize the role of Brat in synaptic development and function, we first examined NMJ morphology in *brat* mutants (Fig. 1). We examined three strong or null alleles *brat[11]*, *brat[150]*,

and *brat¹⁹²*, all nonsense mutations from independent sources (Arama et al., 2000; Frank et al., 2002; Betschinger et al., 2006). These mutant alleles showed no Brat expression by immunostaining and Western blotting (Fig. 2*A,B,E*). Compared with the wild-type, both *brat¹¹/ brat¹⁹²* and *brat¹⁵⁰/brat¹⁹²* mutants exhibited more boutons at muscle 4 NMJ (NMJ 4) on segments A2 and A3. The mean total bouton number in *brat¹¹/ brat¹⁹²* mutants was 55.72 ± 3.13 (mean ± SEM), a 55% increase over the wild-type (35.94 ± 1.86; $p < 0.001$; Fig. 1*A,B,I*), whereas *brat¹⁵⁰/brat¹⁹²* mutants exhibited a similar 46.4% increase compared with wild-type (52.63 ± 3.76, $p < 0.001$; Fig. 1*I*). The number of satellite boutons emanating from the main branch or primary boutons (Dickman et al., 2006; O'Connor-Giles et al., 2008) was significantly higher in mutants (18.00 ± 2.15 for *brat¹¹/brat¹⁹²* mutants, 19.06 ± 2.33 for *brat¹⁵⁰/brat¹⁹²* mutants, 1.63 ± 0.34 for wild-typs; $p < 0.001$ compared with wild-type for both mutants; Fig. 1*I*). To eliminate the possibility that this supernumerary satellite bouton phenotype was caused by a background mutation on the *brat¹⁹²* chromosome, we also examined the NMJ phenotype of *brat¹⁹²* hemizygous mutants (*brat¹⁹²/Df(2L)pr-A16*) and found that they also exhibited excess satellite boutons (data not shown). The excess satellite boutons largely account for the increase in the total bouton number in *brat* mutants.

To confirm that the excess satellite bouton phenotype was caused specifically by *brat* mutations, we examined synaptic terminals in animals where Brat was knocked down by RNA interference driven by the ubiquitous *da-Gal4*. Western analysis confirmed effective Brat knockdown (Fig. 2*E*). As expected, Brat knockdown recapitulated the supernumerary satellite boutons of *brat* mutants (data not shown). Tissue-specific RNAi knockdown was then used to examine whether Brat functions presynaptically or postsynaptically. Targeted RNAi knockdown in presynaptic neurons under control of the pan-neuronal *elav-Gal4* induced an NMJ phenotype similar to that of *brat¹¹/brat¹⁹²* mutants (Fig. 1*B,C,I*). In contrast, postsynaptic knockdown of Brat by the muscle-specific *Mhc-Gal4* did not alter NMJ morphology (Fig. 1*A,D,I*).

To further verify that the distinct NMJ phenotype in *brat* mutants was due to loss of Brat function, we performed tissue-specific rescue experiments using the UAS-Gal4 system (Brand and Perrimon, 1993). We generated a *UAS-flag-brat* transgenic line (Fig. 2*C,D,F*). We observed no obvious rescue of the overgrown phenotype of *brat* mutants when the crosses of *UAS-flag-brat* driven by *elav-Gal4* or *Mhc-Gal4* were cultured at 25°C, probably due to an excess Flag-Brat protein. Indeed, a slightly higher level of Brat than the endogenous level (Fig. 2*F*) could give rise to abnormal NMJs (data not shown), indicating that NMJ growth is sensitive to Brat protein levels. As the Gal4 protein exhibits lower activity at 18°C than that at 25°C (Wucherpfennig et al., 2003; Greenspan, 2004; Harris et al., 2011), we performed
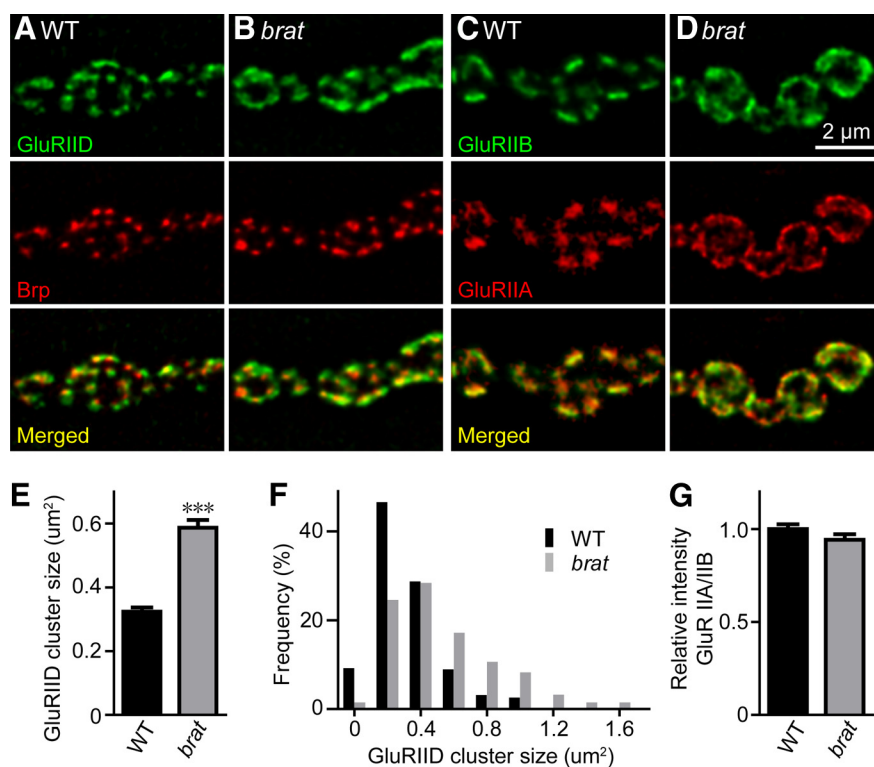

Figure 4. The cluster size of glutamate receptors is increased in *brat* mutants. *A–D*, Confocal images of larval NMJ synapses from wild-type controls and *brat¹¹/brat¹⁹²* mutants double-labeled with anti-GluRIID (green) and anti-Brp (red; *A, B*), and anti-GluRIIB (green) and anti-GluRIIA (red; *C, D*). *E, F*, Statistical results of the mean size (*E*) and size distribution (*F*) of GluRIID clusters (n = 348 for wild-type and n = 338 for *brat* mutants). *G*, Quantification of the ratio of GluRIIA to GluRIIB intensities in controls and *brat¹¹/brat¹⁹²* mutants (n ≥ 15 NMJs). Statistical significance was calculated using Student's *t* test (***$p < 0.001$; error bars denote SEM).

the rescue experiments again at 18°C and found that the satellite bouton number in *brat¹¹/brat¹⁹²* mutants (18.42 ± 2.19) was significantly reduced by the presynaptic expression of *brat* driven by *elav-Gal4* (4.84 ± 0.87; $p < 0.001$; Fig. 1*J*), though not restored to the wild-type level. Motor neuron-specific expression of *brat* driven by *Ok6-Gal4* showed rescue effects (3.31 ± 1.01; $p < 0.001$) similar to that by *elav-Gal4*. In contrast, postsynaptic expression of *brat* driven by *Mhc-Gal4* did not rescue the NMJ deficit ($p > 0.05$; Fig. 1*J*). Neuronal expression of Brat via an independent *UAS-brat* insertion (Sonoda and Wharton, 2001; we confirmed in Fig. 2*E*) produced rescue effects similar to that of *UAS-flag-brat* (data not shown). These tissue-specific RNAi knockdown and rescue experiments demonstrate that Brat regulates NMJ development primarily on the presynaptic side.

Synaptic ultrastructure is altered in *brat* mutants
In addition to light microscopic analyses, we also examined NMJ synapses of *brat* mutants at the ultrastructural level. Presynaptic structures essential for neurotransmitter release at NMJ terminals include mitochondria, SVs, and active zones with T-bars, although the most prominent postsynaptic structure is the subsynaptic reticulum (SSR) composed of a meshwork of convoluted muscle plasma membranes (Fig. 3*A*). The presynaptic mitochondria and postsynaptic SSR appeared largely normal in *brat¹¹/brat¹⁹²* mutants (Fig. 3, compare *B* with *A*). However, the vesicle density within the whole bouton was moderately but significantly reduced (94.71 ± 3.50/μm² in WT vs 82.24 ± 3.31/ μm² in mutants, $p < 0.05$; Fig. 3*G*), although a small subpopulation of vesicles (Fig. 3*B*, arrowheads) were larger in *brat¹¹/brat¹⁹²* mutants compared with the wild-type. There were
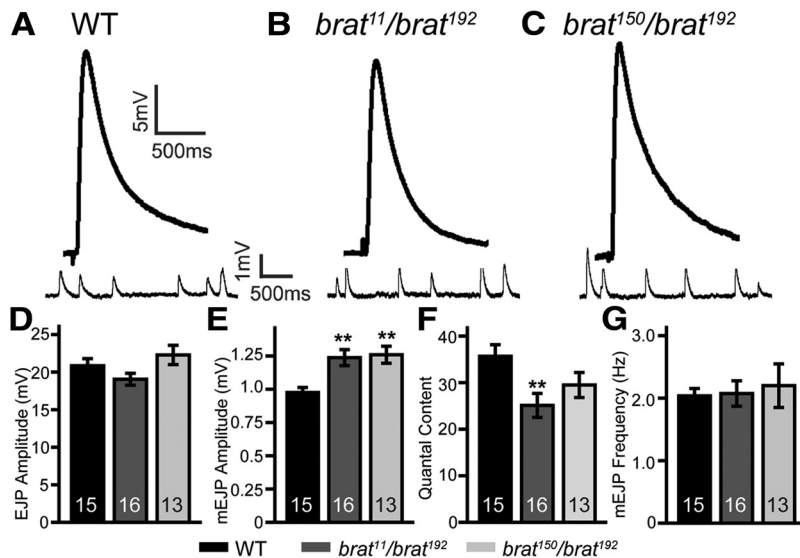
Figure 5. Neurotransmission efficacy is decreased in *brat* mutants. *A–C*, Representative EJP and mEJP traces of wild-type, *brat^11^/brat^192^* and *brat^150^/brat^192^* mutants. *D–G*, Bar graphs showing the statistical results of average EJP amplitude (*D*), mEJP amplitude (*E*), quantal content (*F*), and mEJP frequency (*G*) of different genotypes. The number of animals analyzed for each genotype is indicated in each column. Statistical significance was calculated using one-way ANOVA (**$p < 0.01$; error bars denote SEM).
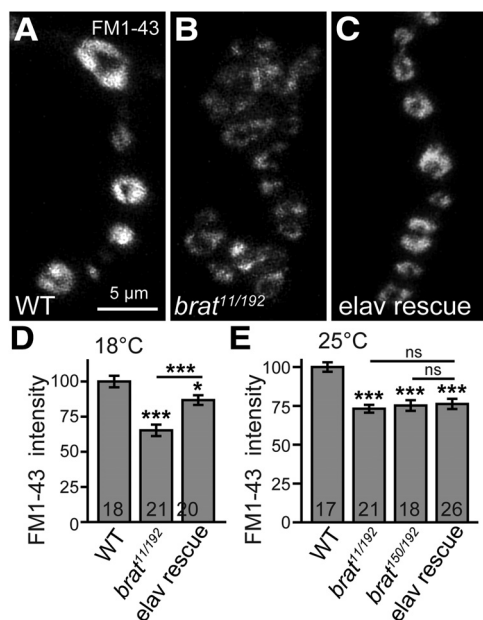

Figure 6. Brat is required for the normal FM1-43 uptake at NMJ terminals. *A–E*, FM1-43 uptake results performed at 18°C (*A–D*) and 25°C (*E*). The wild-type synapses were labeled brightly by endocytosed FM1-43 at 18°C (*A*). In contrast, *brat^11^/brat^192^* mutants (*B*) showed a significant reduction in the fluorescent intensity of endocytosed FM1-43. The reduced FM1-43 intensity in *brat* mutants was partially rescued by presynaptic expression of *brat* at 18°C (*C*, *elav-Gal4/+*; *brat^11^/brat^192^*; *UAS-flag-brat/+*). Scale bar, 5 μm. *D*, *E*, Statistical results of relative intensities of loaded FM1-43 dye in different genotypes at 18°C (*D*) and 25°C (*E*). Statistical significance was calculated using one-way ANOVA (*$p < 0.05$; **$p < 0.01$; ***$p < 0.001$; error bars denote SEM).

mutants compared with wild-type (40.33 ± 0.43 nm vs 30.67 ± 0.28 nm; $p < 0.001$; Fig. 3*E,F,K*). A histogram and cumulative probability plot showed that 91% of wild-type SVs were <40 nm, compared with only 55% of SVs in *brat^11^/brat^192^* mutants (Fig. 3*L,M*). Hence, loss of Brat reduced vesicle density but resulted in a subpopulation of larger vesicles at NMJ terminals, a phenotype similar to that observed in many endocytic mutants, such as *AP180/lap*, *dap160*, and *tweek* (Zhang et al., 1998; Koh et al., 2004; Verstreken et al., 2009). The larger SVs may contain more glutamate neurotransmitter, consistent with the greater amplitudes of spontaneous mEJP in *brat* mutants (Fig. 5; see below). We also observed a significant increase in the number of presynaptic membrane ruffles within the electron-dense membranes at the AZ in *brat* mutants (0.41 ± 0.06 ruffles per AZ for *brat^11^/brat^192^* mutants vs 0.04 ± 0.02 ruffles per AZ for the wild-type; Fig. 3*I*), suggesting a defect in endocytosis, cell adhesion, or both.

The mean length of the postsynaptic density (PSD; Fig. 3*C,D*, arrowheads) where glutamate receptors are enriched was longer in *brat* mutants compared with wild-type (1.06 ± 0.05 μm vs 0.56 ± 0.02 μm; $p < 0.001$; Fig. 3*H*), consistent with immunostaining results showing an enlarged cluster size of GluRIID, an obligatory subunit of functional receptors (Featherstone et al., 2005; Qin et al., 2005), in *brat* mutants (0.32 ± 0.13 μm² in WT vs 0.58 ± 0.25 μm² in *brat^11^/brat^192^* mutants, $p < 0.001$; Fig. 4*A,B,E,F*). We observed similar enlarged cluster size of GluR subunits IIA and IIB (Fig. 4*C,D*), but the ratio of GluRIIA to GluRIIB intensities was normal in *brat* mutants (Fig. 4*G*).

brat mutants show increased quantal size but decreased neurotransmission efficacy at NMJ terminals

To examine the functional consequences of these altered NMJ synapses in *brat* mutants, we recorded EJPs and spontaneous mEJPs at NMJ 6/7 using intracellular electrodes. In 0.23 mM Ca²⁺ HL3.1 saline, neither mean EJP amplitude (19.06 ± 0.79 mV for *brat^11^/brat^192^*, 22.29 ± 1.28 mV for *brat^150^/brat^192^* vs 20.86 ± 0.94 mV for wild-type; Fig. 5*A–D*) nor mEJP frequency (2.07 ± 0.20 Hz for *brat^11^/brat^192^*, 2.20 ± 0.35 Hz for *brat^150^/brat^192^* vs 2.04 ± 0.12 Hz for wild-type; Fig. 5*A–C,G*) was significantly altered in *brat* mutants ($p > 0.05$). However, the mean mEJP amplitude was significantly larger in *brat* mutants (1.24 ± 0.06 mV for *brat^11^/brat^192^*, 1.26 ± 0.06 mV for *brat^150^/brat^192^* vs 0.98 ± 0.04 mV for wild-type; $p < 0.01$ for both; Fig. 5*E*), consistent with the larger synaptic vesicles that presumably contain more glutamate in *brat* mutant boutons (Fig. 3). The enlarged GluR cluster size (Fig. 4) may also contribute to the increased mEJP amplitudes in *brat* mutants.

The number of vesicles released per stimulus (quantal content) is a measure of synaptic transmission efficacy and is calculated by dividing EJP amplitude (after correction for nonlinear summation) by mEJP amplitude. The estimated quantal content in heteroallelic *brat^150^/brat^192^* mutants was reduced, but not significantly different from wild-type ($p > 0.05$; Fig. 5*F*), whereas that in *brat^11^/brat^192^* mutants was significantly lower compared

also fewer synaptic vesicles within a 200 nm radius of the T-bar in *brat^11^/brat^192^* mutants (16.31 ± 0.62) than wild-type (21.13 ± 0.91; $p < 0.001$; Fig. 3*E,F,J*). The mean SV diameter within the area of active zones (AZs) was significantly larger in *brat^11^/brat^192^*

with the wild-type (25.10 ± 2.58 quanta/stimulus vs 36.28 ± 2.60 quanta/stimulus for wild-type; $p < 0.01$; Fig. 5F). The weaker phenotype of the $brat^{150}/brat^{192}$ mutant is consistent with the molecular nature of the mutation; $brat^{150}$ is a nonsense mutation resulting in the C-terminal 112 aa region deleted, whereas $brat^{11}$ has a larger 259 aa C-terminal deletion (Arama et al., 2000; Betschinger et al., 2006). These results show that $brat$ mutants have a larger quantal size but decreased neurotransmission efficacy at NMJ synapses.

Synaptic endocytosis is impaired in *brat* mutants

In *brat* mutants, the NMJ terminals show excessive satellite boutons, reduced vesicle density but increased vesicle size at AZs, increased mEJP amplitudes, and lower transmission efficiency (Figs. 1, 3–5). Similar synaptic defects were observed in many endocytic mutants, such as *AP180*, *dap160*, *dynamin*, and *endophilin* (Zhang et al., 1998; Verstreken et al., 2002; Koh et al., 2004; Marie et al., 2004; Dickman et al., 2006), we therefore examined whether *brat* regulates synaptic vesicle endocytosis using the lipophilic fluorescent dye FM1-43. At *Drosophila* NMJ terminals, FM1-43 binds to synaptic membranes, is internalized during endocytosis, and gets trapped in synaptic vesicles, where its fluorescence can be measured after washout of extracellular dye, providing a measure of endocytic efficiency (Verstreken et al., 2008; Wang et al., 2010). Dissected larvae were stimulated with 90 mM KCl for 5 min in the presence of 10 μM FM1-43 to induce transmitter release and concomitant endocytosis of the dye. After washing with Ca^{2+}-free saline, the accumulated FM1-43 in live NMJ 4 synapses was imaged by confocal microscopy. Compared with wild-type NMJ boutons, *brat* mutant boutons exhibited significantly lower FM1-43 fluorescence at 25°C (73.2% and 75.2% of the wild-type fluorescence intensity in $brat^{11}/brat^{192}$ and $brat^{150}/brat^{192}$ mutants, respectively; $p < 0.001$; Fig. 6E). However, the reduced FM1-43 intensity in *brat* mutants was not rescued by the presynaptic expression of *flag-brat* at 25°C (Fig. 6E), probably due to an inappropriate protein level of Flag-Brat. We then cultured the crosses at 18°C, which allowed for a lower Brat expression from *elav-Gal4>UAS-flag-brat* and better rescue for NMJ phenotypes (Fig. 1). Under these conditions, the relative intensity of FM1-43 fluorescence in $brat^{11}/brat^{192}$ mutants was 65.2% of wild-type intensity at 18°C ($p < 0.001$; Fig. 6A,B,D) and was partially but significantly rescued to 86.77% of the wild-type by the presynaptic expression of *brat* ($p < 0.001$; Fig. 6C,D), indicating an endocytic defect at *brat* NMJ terminals.

Figure 7. Synaptic overgrowth in *brat* mutants is rescued by decreasing the dose of *mad*. **A–J**, Confocal images of NMJ 4 double-labeled with anti-CSP (green) and anti-HRP (red). Wild-type (**A**), $brat^{11}/brat^{192}$ (**B**), $tkv^7/+$ (**C**), $Df(2L)162/+$ (**D**), and $dad^{J1E4}/+$ (**E**) showed normal NMJ morphology. **F, G**, Removing one copy of *wit* or *tkv* did not suppress the synaptic overgrowth in *brat* mutants. The genotypes are $brat^{11}/brat^{192}$; $wit^{A12}/+$ (**F**) and $brat^{11}/brat^{192}$; $tkv^7/+$ (**G**). **H, I**, Removing one copy of *mad* rescued synaptic overgrowth of *brat* mutants to the wild-type level. The genotypes are $brat^{11}/brat^{192}$; $mad^{12}/+$ (**H**) and $brat^{11}/brat^{192}$; $Df(2L)162/+$ (**I**). **J**, Trans-heterozygous $brat^{192}/+$; $dad^{J1E4}/+$ mutants showed more satellite boutons compared with wild-type. Scale bar, 10 μm. **K, L**, Quantification of total bouton number (**K**) and satellite bouton number (**L**) of NMJ 4 for various genotypes. Statistical significance was calculated using one-way ANOVA ($n \geq 15$ NMJs; **$p < 0.01$; ***$p < 0.001$; error bars denote SEM).

rescued by the presynaptic expression of *flag-brat* at 25°C (Fig. 6E), probably due to an inappropriate protein level of Flag-Brat. We then cultured the crosses at 18°C, which allowed for a lower Brat expression from *elav-Gal4>UAS-flag-brat* and better rescue for NMJ phenotypes (Fig. 1). Under these conditions, the relative intensity of FM1-43 fluorescence in $brat^{11}/brat^{192}$ mutants was 65.2% of wild-type intensity at 18°C ($p < 0.001$; Fig. 6A,B,D) and was partially but significantly rescued to 86.77% of the wild-type by the presynaptic expression of *brat* ($p < 0.001$; Fig. 6C,D), indicating an endocytic defect at *brat* NMJ terminals.
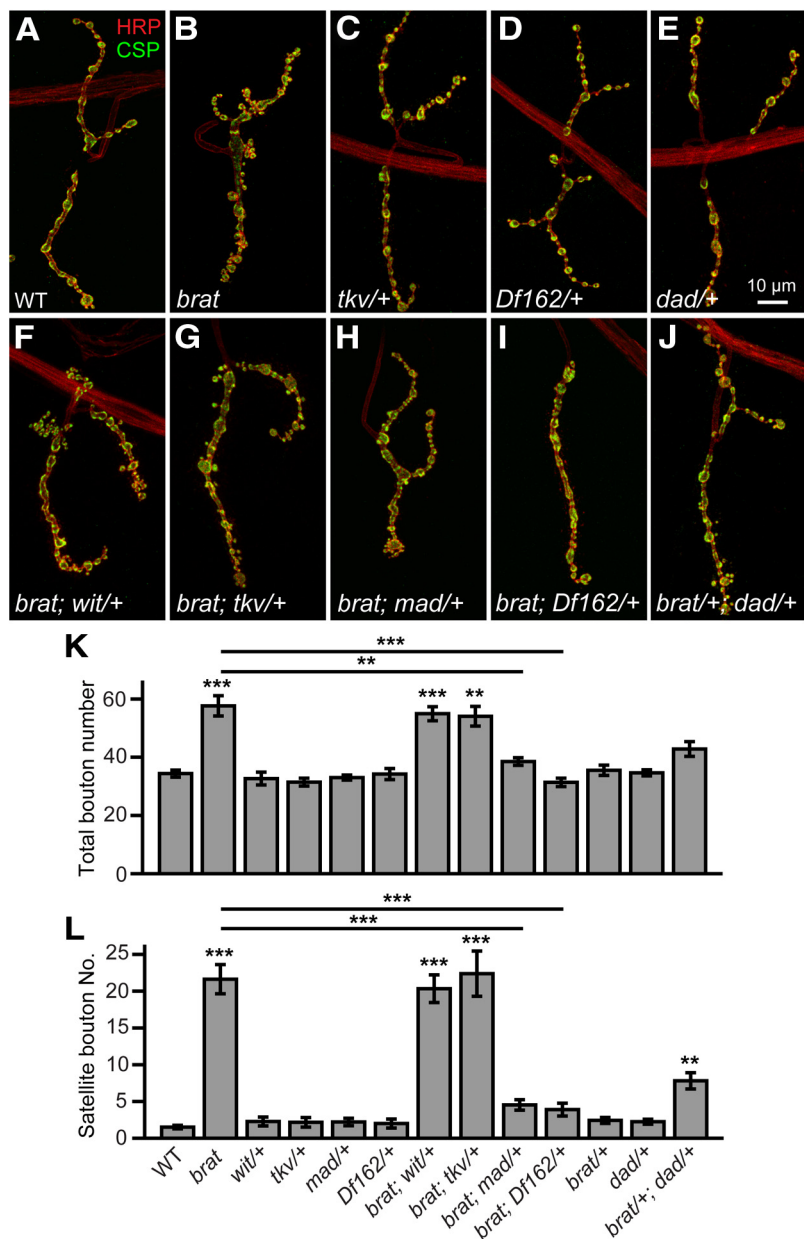
Synaptic defects of *brat* mutants are rescued by reducing the dose of *mad*

Brat suppresses the translation of the BMP signaling molecule Mad during germline development (Harris et al., 2011) and enhanced BMP signaling leads to the development of excess satellite boutons at NMJs (Sweeney and Davis, 2002; Collins and DiAntonio, 2007; O'Connor-Giles et al., 2008; Zhao et al., 2013). These findings suggest that the effects of loss of Brat function at NMJ terminals may be mediated by BMP hyperactivation. We therefore examined synaptic overgrowth in *brat* mutants with reduced
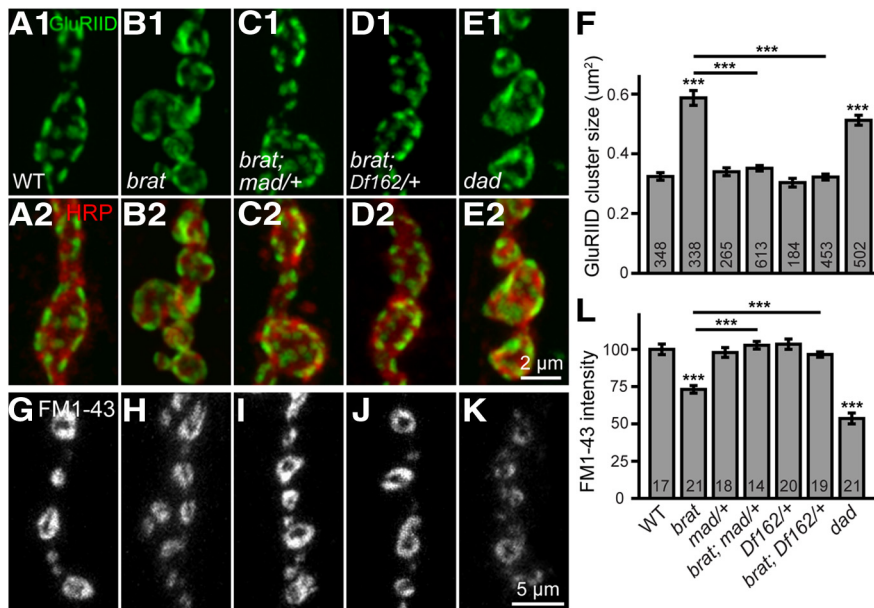
Figure 8. Enlarged GluRIID cluster size and defective endocytosis in *brat* mutants are rescued by reducing the dose of *mad*. **A–E,** Confocal images of NMJ 4 boutons double-labeled with anti-GluRIID (green) and anti-HRP (red). The enlarged GluRIID cluster size in *brat¹¹/brat¹⁹²* mutants (**B**) was fully rescued by *mad¹²/+* (**C**) and *Df(2L)162)/+* (**D**) to wild-type. **E,** A homozygous hypomorphic *dad^{J1E4}* also caused enlarged GluRIID cluster size. **F,** Quantification of GluRIID cluster size of different genotypes. The number of GluRIID cluster analyzed for each genotype is indicated in the columns. **G–K,** FM1-43 uptake at NMJ 4 of different genotypes. The genotypes are **G**, wild-type, **H**, *brat¹¹/brat¹⁹²*, **I**, *brat¹¹/brat¹⁹²; mad¹²/+*, **J**, *brat¹¹/brat¹⁹²; (Df(2L)162)/+*, and **K**, *dad^{J1E4}*. **L,** Statistical results of relative intensities of loaded FM1-43 dye at NMJ boutons of different genotypes. Scale bars: **E1**, 2 μm; **K**, 5 μm. The number of animals analyzed for each genotype is indicated in the columns. Statistical significance was calculated using one-way ANOVA (***$p < 0.001$; error bars denote SEM).

BMP signaling. Mutating one copy of *wit* (*wit^{A12}*) or *tkv* (*tkv⁷*) had no effect on NMJ growth and did not rescue the overgrowth of NMJs in *brat* mutants ($p > 0.05$; Fig. 7C,F,G,K,L), suggesting that synaptic overgrowth in *brat* mutants is independent of the dose of the BMP receptors Wit or Tkv. However, removal of one copy of *mad* (heterozygous *mad¹²* or deletion *Df(2L)162* that uncovers *mad*) had no effect on NMJ growth on the wild-type genetic background but significantly suppressed the excess bouton and satellite bouton phenotype of *brat* mutants (for satellite bouton, 4.53 ± 0.71 for *brat¹¹/brat¹⁹²*; *mad¹²/+*, 3.90 ± 0.87 for *brat¹¹/brat¹⁹²*; *Df(2L)162)/+* vs 21.63 ± 1.95 for *brat¹¹/brat¹⁹²*; Fig. 7D,H,I,K,L). Conversely, *trans*-heterozygotes of *brat¹⁹²* and *dad^{J1E4}* (*dad* encodes an inhibitory Smad that negatively regulates BMP signaling) showed significantly more satellite boutons compared with wild-type, whereas the single heterozygous *brat¹⁹²* or *dad^{J1E4}* mutants showed normal NMJ morphology (Fig. 7E,J,L). Together, these results indicate that synaptic overgrowth in *brat* mutants may result from increased *mad* activity, consistent with Western results showing that Mad protein level was upregulated in *brat* mutants (see Fig. 9).

brat not only regulates NMJ development, but also affects the cluster size of glutamate receptors and endocytosis (Figs. 3, 4, 6). We therefore examined whether *mad* played a role in these *brat*-regulated processes. Both *brat* and *dad* mutants exhibited larger postsynaptic clusters of GluRIID receptors and endocytosis defects. Reducing the dose of *mad* by half in heterozygous *mad¹²* or *Df(2L)162* mutants reversed the enlarged GluRIID cluster size (Fig. 8A–D,F) and the reduced FM1-43 dye uptake in *brat¹¹/brat¹⁹²* mutants to wild-type levels (Fig. 8G–J,L), suggesting that changes in the cluster size of glutamate receptors and reduced endocytosis in *brat* mutants are caused by increased *mad* expression. This notion was further supported by the fact that FM1-43 uptake was significantly

reduced in homozygous hypomorphic *dad^{J1E4}* mutants compared with wild-type (Fig. 8G,K,L).

Reducing *mad* expression was sufficient to reverse the principal aberrant NMJ phenotypes in *brat* mutants, including supernumerary satellite boutons, enlarged glutamate receptor clusters, and reduced endocytosis, indicating that the functions of *brat* in NMJ development are mediated through *mad*.

Mad protein level is increased in *brat* mutants

We then examined whether the protein level of Mad was altered in *brat* mutants. Mad is an effector of BMP signaling and the phosphorylated Mad (pMad) level serves as a molecular read out of BMP signaling at NMJ terminals (Wang et al., 2007; O'Connor-Giles et al., 2008). The pMad intensity normalized to HRP intensity was dramatically elevated in *brat¹¹/brat¹⁹²* mutant NMJ synapses compared with the wild-type ($p < 0.001$; Fig. 9A,B,E). Tissue-specific rescue experiments using different *Gal4* drivers showed that presynaptic expression of Flag-Brat driven by *elav-Gal4* rescued the elevated pMad staining at *brat¹¹/brat¹⁹²* mutant NMJs concomitant with a reduction in satellite bouton number (Fig. 9A2–C2), whereas postsynaptic (muscular) expression of Flag-Brat under the control of *Mhc-Gal4* did not significantly rescue *brat* mutant NMJ phenotypes (Fig. 9B,D,E). Consistent with the elevated pMad level at NMJs, pMad level was also upregulated in motor neuron nuclei of *brat* mutants (Fig. 9F–J).

Western analysis of larval brains demonstrated that the protein level of Mad in larval brains was higher in *brat* mutants and RNAi knockdown animals (4.24-fold increase for *brat¹¹/brat¹⁹²*, 4.41-fold increase for *brat¹⁵⁰/brat¹⁹²*, and 2.18-fold increase for *brat^{RNAi}* compared with wild-type; Fig. 9K,M). The pMad protein level also had a similar increase in *brat* mutants (Fig. 9K,M). The specificities of the anti-pMad and anti-Mad antibodies were verified by the reduced Mad and pMad band intensities on Western blots when *mad* expression was knocked down by RNA interference (RNAi; Fig. 9K). We observed that increased expression of Mad protein also led to an elevated level of pMad on the wild-type background (data not shown). Knockdown of *brat* by RNAi in S2 cells also led to a twofold increased Mad and pMad proteins (Fig. 9K,M). In contrast, quantitative PCR showed normal *mad* mRNA level in *brat* mutant brains, whereas a significant reduction in *mad* mRNA level was observed when *mad* RNAi was expressed under the control of the ubiquitous *da-Gal4* promoter (Fig. 9L). Elevated levels of pMad and Mad proteins with normal *mad* mRNA expression in *brat* mutants indicate that Brat likely inhibits Mad translation.

Discussion
Brat regulates synapse growth
Brain tumor (*brat*) was first identified as a tumor suppressor in *Drosophila* (Gateff, 1978) and it is now known that Brat acts together with translational repressors Pum and Pum-Nos complex in multiple developmental contexts. It is also known that

Pum and Nos play critical but distinct roles in NMJ synapse development and function. Boutons are larger and fewer in *pum* mutants, whereas neuronal *pum* overexpression leads to smaller and more numerous boutons (Menon et al., 2004). Pum selectively binds to the 3′ untranslated regions of Nanos mRNA, eIF-4E mRNA, and GluR IIA mRNA, and thereby suppresses translation of the encoded proteins at NMJ synapses (Menon et al., 2004, 2009). *nanos* mutants show more boutons, significantly decreased expression of GluR IIA, and increased expression of GluR IIB (Menon et al., 2009). Through a series of elegant genetic, immunohistochemical, and biochemical experiments, Menon et al. (2009) propose an intricate regulatory network among Pumilio, Nanos, and their targets at *Drosophila* NMJ synapses.

Unlike Pum and Nos, which are localized neuronal cell bodies and at NMJ terminals (Menon et al., 2004, 2009), we detected enriched expression of Brat in the neuronal soma (Fig. 2), but no endogenous Brat or ectopically expressed, functional Flag-Brat at NMJ synapses by immunostaining (data not shown). However, Olesnicky et al. (2012) reported that Brat is localized at presynaptic NMJ terminals. They also reported fewer boutons in *brat* mutants rather than excess satellite boutons as we observed (Fig. 1), possibly due to the different antibodies and quantification methods used. The conflicts between their study and the present study remain to be addressed. However, in agreement with their study, we also found that Brat regulated NMJ synapse development on the presynaptic side (Fig. 1).

In the present study, we found that *brat* mutants exhibit an NMJ phenotype distinct from that of *pum* and *nos* mutants, characterized by excess satellite boutons (Fig. 1), reduced transmitter release efficiency (Fig. 5), and defective endocytosis (Fig. 6). Satellite boutons are small boutons that protrude from synaptic branches or from a larger parent bouton. Mutations in genes involved in endocytosis (Dickman et al., 2006), TGFβ/BMP signaling (O'Connor-Giles et al., 2008; Nahm et al., 2010a,b), actin cytoskeleton dynamics (Coyle et al., 2004; Rodal et al., 2008; Ball et al., 2010; Nahm et al., 2010a,b), neuronal excitability (Lee and Wu, 2010), and several other processes (Khodosh et al., 2006; Korolchuk et al., 2007; Yao et al., 2009; Schulte et al., 2010) all lead to prominent satellite boutons at NMJ terminals. Many of these processes and signaling pathways closely interact, thus accounting for the common satellite phenotype of many mutants. For example, endocytosis attenuates BMP signaling (O'Connor-Giles et al., 2008) and
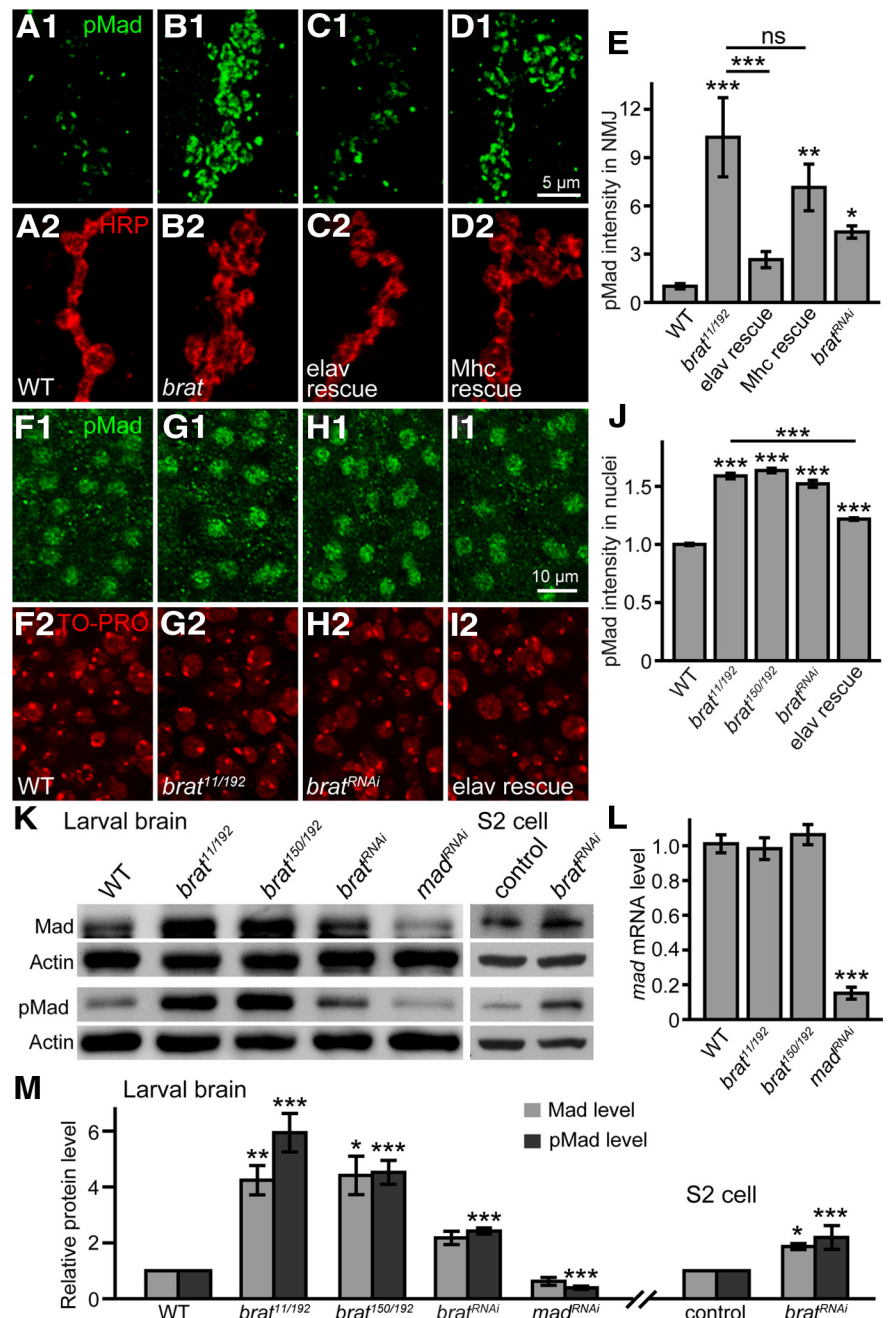

Figure 9. *brat* represses *mad* expression post-transcriptionally. ***A–D***, Confocal images of NMJ 4 colabeled with anti-pMad (green) and anti-HRP (red). ***A***, pMad staining in wild-type NMJ. ***B***, pMad level was dramatically upregulated in *brat[11]*/*brat[192]* mutants compared with wild-type. ***C, D***, The upregulated pMad level in *brat* mutants was partially rescued by neuronal (***C***) but not muscular (***D***) expression of Flag-Brat. ***E***, Quantification of the intensity of pMad levels normalized to the anti-HRP staining intensity at NMJ terminals ($n \geq 10$ NMJs). ***F–I***, Confocal images of motor neuron nuclei in third-instar larval VNCs double-stained with anti-pMad (green) and TO-PRO-3 iodide (red). The genotypes are wild-type (***F***), *brat[11]*/*brat[192]* (***G***), *UAS-mad[RNAi]*/+; *da-Gal4*/+ (***H***), and *elav-Gal4*/+; *brat[11]*/*brat[192]*; *UAS-flag-brat*/+ (***I***). ***J***, Quantification of pMad intensities in motor neuron nuclei of different genotypes ($n \geq 100$ motor neurons from at least eight larvae). Scale bars: ***D1***, 5 μm; ***I1***, 10 μm. ***K***, Western results of endogenous Mad and pMad proteins from larval brains of wild-type, *brat[11]*/*brat[192]*, *brat[150]*/*brat[192]*, and *UAS-mad[RNAi]*/+; *da-Gal4*/+, and from S2 cells treated with *brat RNAi*. ***L***, Normalized levels of *mad* mRNAs determined using real-time PCR from larval brains of different genotypes. ***M***, Statistical results of Mad and pMad protein levels in the larval brains of *brat* mutants and S2 cells where *brat* was knocked down by RNAi ($n \geq 5$; *$p < 0.05$; **$p < 0.01$; ***$p < 0.001$; error bars denote SEM).

BMP signaling affects bouton formation via regulating actin dynamics by promoting the transcription of Trio, a Rac GTPase guanine exchange factor (Ball et al., 2010). As we discuss below, Brat may suppress satellite bouton formation by inhibiting BMP signaling.

Brat normally suppresses Mad expression to regulate synaptic growth

Brat is a translational repressor containing no RNA-binding domains. During embryonic development, Brat suppresses mRNA translation by interacting with the RNA-binding proteins Pum and Nanos (Sonoda and Wharton, 2001; Cho et al., 2006). In the female germline, Brat acts with Pum to promote stem-cell differentiation by inhibiting target gene translation (Harris et al., 2011). In the nervous system, Brat is required for Pumilio-Nanos-dependent repression of the voltage-gated sodium channel subunit gene *para* in motoneurons, but dispensable for the negative regulation of *para* by the Pumilio-Nanos complex in other neuronal types (Muraro et al., 2008). It remains to be determined whether Brat interacts with Pumilio and Nanos to regulate genes involved in NMJ synapse growth. The distinct NMJ phenotypes between *brat* mutants and *pum* and *nos* mutants indicate that *brat* may regulate synapse development independently of *pum* and *nos* on the postsynaptic side. In support of their independent functions at postsynaptic NMJ synapses, *brat* mutants showed normal levels of GluRIIA and IIB (Fig. 4), whereas the level of GluRIIA and GluRIIB is upregulated in *pum* and *nos* mutant NMJ terminals, respectively (Menon et al., 2004, 2009). However, on the presynaptic side, our results showed that pMAD level was dramatically increased in *pum¹* null mutants; *trans*-heterozygous *pum¹*/+; *brat¹⁹²*/+ mutants also showed an increased pMad level at NMJ synapses (data not shown). These results suggest that Mad might be repressed by the Pum-Brat complex in presynaptic neurons, consistent with a previous finding of inhibition of *mad* by the Pum-Brat complex in S2 cells (Harris et al., 2011).

The major NMJ phenotypes of *brat* mutants, including excess satellite boutons, increased GluR cluster size, and endocytic defects (Figs. 1, 4, 6), were rescued by decreasing the dose of the BMP signaling effector Mad (Figs. 7, 8). Both pMad and total Mad protein expression levels were higher, whereas *mad* mRNA expression was normal in the larval brains of *brat* mutants (Fig. 9). Furthermore, Brat knockdown by RNA interference in S2 cells also led to increased expression of Mad and pMad (Fig. 9). These results indicate that Brat normally acts to limit BMP signaling by suppressing the translation of Mad mRNA. In support of this conclusion, Brat specifically suppresses Mad translation via its 3′ untranslated region in S2 cells (Harris et al., 2011). The negative regulation of Mad by Brat in the nervous system is reminiscent of that described in ovarian stem-cell differentiation (Harris et al., 2011), suggesting that this is a conserved mechanism for BMP signaling regulation.

A significantly increased cluster size of glutamate receptors in *brat* mutants, as well as in *dad* mutants (Figs. 4, 8), indicating that the aberrantly elevated BMP signaling might lead to changes in postsynaptic receptor organization. Moreover, the enlarged GluR cluster size of *brat* mutants was completely reversed by heterozygous *mad* mutations (Fig. 8). How might Brat, which appears to act in presynaptic neurons, control postsynaptic GluR cluster size? Elevated BMP signaling may lead to abnormal F-actin dynamics at the presynaptic terminals via enhanced expression of Trio (Ball et al., 2010), but it is unknown whether altered presynaptic F-actin could contribute to the increased GluR cluster size on the postsynaptic side. However, two *trans*-synaptic complexes, neuroligin 1–neurexin and teneurins, have been reported to restrict GluR cluster size (Pielage et al., 2006; Li et al., 2007; Banovic et al., 2010;

Mosca et al., 2012). Furthermore, both neuroligin and teneurins are required to maintain the postsynaptic spectrin cytoskeleton (Mosca et al., 2012). Thus, it is conceivable that BMP signaling, negatively regulated by Brat through Mad, may affect one or both of these *trans*-synaptic signaling pathways. Alternatively, an as yet unidentified Brat target may regulate the postsynaptic cytoskeleton and the postsynaptic architecture.

Brat regulates synaptic endocytosis by suppressing BMP signaling

We provide multiple lines of independent evidence supporting that *brat* regulates synaptic endocytosis. First, *brat* mutants show excess satellite boutons, which are a general feature of endocytic mutants, such as *dap160*, *endophilin*, and *eps15* (Koh et al., 2004, 2007; Dickman et al., 2006). Second, the NMJ boutons in *brat* mutants exhibited other abnormal characteristics of endocytic mutants, including larger but fewer vesicles (Fig. 3) and a concomitant increase in mEJP amplitudes (Fig. 5). Third, as with *tweek*, *dap160*, and *twf* mutants with defective endocytosis (Koh et al., 2004; Verstreken et al., 2009; Wang et al., 2010), the FM1-43 dye uptake was reduced at *brat* mutant NMJ (Fig. 6).

brat mutations led to endocytic defects as well as increased BMP signaling. Increased BMP signaling leads to excess satellite boutons (O'Connor-Giles et al., 2008), but it has not been known whether upregulation of BMP signaling results in endocytic defects. We show here that the endocytic defect in *brat* mutants could be rescued by reducing the dose of *mad*. Moreover, multiple mutations in *dad*, a negative regulator of BMP signaling, resulted in excess satellite boutons and reduced FM1-43 dye uptake at NMJ terminals (Fig. 8; O'Connor-Giles et al., 2008). Thus, increased BMP signaling can result in endocytic defects, probably by affecting actin cytoskeleton, as Trio, a Rac GTPase guanine exchange factor, is a direct target of Mad (Ball et al., 2010). As endocytic defects lead to increased BMP signaling (O'Connor-Giles et al., 2008), there seems a mutual negative regulation between endocytosis and BMP signaling, i.e., a positive feedback loop for BMP signaling, at NMJ terminals.

In summary, our results provide genetic and biochemical evidence for a model in which Brat regulates synaptic growth and endocytosis at NMJ terminals by suppressing the translation of Mad, an effector of BMP signaling. This study describes a previously unknown regulatory mechanism for BMP signaling in the nervous system.

References

Arama E, Dickman D, Kimchie Z, Shearn A, Lev Z (2000) Mutations in the beta-propeller domain of the *Drosophila* brain tumor (*brat*) protein induce neoplasm in the larval brain. Oncogene 19:3706–3716. CrossRef Medline

Ball RW, Warren-Paquin M, Tsurudome K, Liao EH, Elazzouzi F, Cavanagh C, An BS, Wang TT, White JH, Haghighi AP (2010) Retrograde BMP signaling controls synaptic growth at the NMJ by regulating trio expression in motor neurons. Neuron 66:536–549. CrossRef Medline

Banovic D, Khorramshahi O, Owald D, Wichmann C, Riedt T, Fouquet W, Tian R, Sigrist SJ, Aberle H (2010) *Drosophila* neuroligin 1 promotes growth and postsynaptic differentiation at glutamatergic neuromuscular junctions. Neuron 66:724–738. CrossRef Medline

Bayat V, Jaiswal M, Bellen HJ (2011) The BMP signaling pathway at the *Drosophila* neuromuscular junction and its links to neurodegenerative diseases. Curr Opin Neurobiol 21:182–188. CrossRef Medline

Bello B, Reichert H, Hirth F (2006) The *brain tumor* gene negatively regulates neural progenitor cell proliferation in the larval central brain of *Drosophila*. Development 133:2639–2648. CrossRef Medline

Betschinger J, Mechtler K, Knoblich JA (2006) Asymmetric segregation of the tumor suppressor brat regulates self-renewal in *Drosophila* neural stem cells. Cell 124:1241–1253. CrossRef Medline

Brand AH, Perrimon N (1993) Targeted gene expression as a means of altering cell fates and generating dominant phenotypes. Development 118: 401–415. Medline

Cho PF, Gamberi C, Cho-Park YA, Cho-Park IB, Lasko P, Sonenberg N (2006) Cap-dependent translational inhibition establishes two opposing morphogen gradients in *Drosophila* embryos. Curr Biol 16: 2035–2041. CrossRef Medline

Collins CA, DiAntonio A (2007) Synaptic development: insights from *Drosophila*. Curr Opin Neurobiol 17:35–42. CrossRef Medline

Coyle IP, Koh YH, Lee WC, Slind J, Fergestad T, Littleton JT, Ganetzky B (2004) Nervous wreck, an SH3 adaptor protein that interacts with Wsp, regulates synaptic growth in *Drosophila*. Neuron 41:521–534. CrossRef Medline

Dickman DK, Lu Z, Meinertzhagen IA, Schwarz TL (2006) Altered synaptic development and active zone spacing in endocytosis mutants. Curr Biol 16:591–598. CrossRef Medline

Edwards TA, Wilkinson BD, Wharton RP, Aggarwal AK (2003) Model of the brain tumor-pumilio translation repressor complex. Genes Dev 17: 2508–2513. CrossRef Medline

Eivers E, Fuentealba LC, Sander V, Clemens JC, Hartnett L, De Robertis EM (2009) Mad is required for wingless signaling in wing development and segment patterning in *Drosophila*. PloS One 4:e6543. CrossRef Medline

Featherstone DE, Rushton E, Rohrbough J, Liebl F, Karr J, Sheng Q, Rodesch CK, Broadie K (2005) An essential *Drosophila* glutamate receptor subunit that functions in both central neuropil and neuromuscular junction. J Neurosci 25:3199–3208. CrossRef Medline

Frank DJ, Edgar BA, Roth MB (2002) The *Drosophila melanogaster* gene *brain tumor* negatively regulates cell growth and ribosomal RNA synthesis. Development 129:399–407. Medline

Gateff E (1978) Malignant neoplasms of genetic origin in *Drosophila melanogaster*. Science 200:1448–1459. CrossRef Medline

Giagtzoglou N, Ly CV, Bellen HJ (2009) Cell adhesion, the backbone of the synapse: "vertebrate" and "invertebrate" perspectives. Cold Spring Harb Perspect Biol 1:a003079. CrossRef Medline

Greenspan RJ (2004) Fly pushing: the theory and practice of *Drosophila* genetics. Cold Spring Harbor, NY: CSHL.

Harris RE, Pargett M, Sutcliffe C, Umulis D, Ashe HL (2011) Brat promotes stem cell differentiation via control of a bistable switch that restricts BMP signaling. Dev Cell 20:72–83. CrossRef Medline

Jan LY, Jan YN (1976) Properties of the larval neuromuscular junction in *Drosophila melanogaster*. J Physiol 262:189–214. Medline

Jin S, Pan L, Liu Z, Wang Q, Xu Z, Zhang YQ (2009) *Drosophila* Tubulin-specific chaperone E functions at neuromuscular synapses and is required for microtubule network formation. Development 136:1571–1581. CrossRef Medline

Khodosh R, Augsburger A, Schwarz TL, Garrity PA (2006) Bchs, a BEACH domain protein, antagonizes Rab11 in synapse morphogenesis and other developmental events. Development 133:4655–4665. CrossRef Medline

Koh TW, Verstreken P, Bellen HJ (2004) Dap160/intersectin acts as a stabilizing scaffold required for synaptic development and vesicle endocytosis. Neuron 43:193–205. CrossRef Medline

Koh TW, Korolchuk VI, Wairkar YP, Jiao W, Evergren E, Pan H, Zhou Y, Venken KJ, Shupliakov O, Robinson IM, O'Kane CJ, Bellen HJ (2007) Eps15 and Dap160 control synaptic vesicle membrane retrieval and synapse development. J Cell Biol 178:309–322. CrossRef Medline

Korolchuk VI, Schütz MM, Gómez-Llorente C, Rocha J, Lansu NR, Collins SM, Wairkar YP, Robinson IM, O'Kane CJ (2007) *Drosophila* Vps35 function is necessary for normal endocytic trafficking and actin cytoskeleton organisation. J Cell Sci 120:4367–4376. CrossRef Medline

Lee CY, Wilkinson BD, Siegrist SE, Wharton RP, Doe CQ (2006) Brat is a Miranda cargo protein that promotes neuronal differentiation and inhibits neuroblast self-renewal. Dev Cell 10:441–449. CrossRef Medline

Lee J, Wu CF (2010) Orchestration of stepwise synaptic growth by K+ and Ca^{2+} channels in *Drosophila*. J Neurosci 30:15821–15833. CrossRef Medline

Li J, Ashley J, Budnik V, Bhat MA (2007) Crucial role of *Drosophila* neurexin in proper active zone apposition to postsynaptic densities, synaptic growth, and synaptic transmission. Neuron 55:741–755. CrossRef Medline

Liu Z, Huang Y, Zhang Y, Chen D, Zhang YQ (2011) *Drosophila* acyl-CoA synthetase long-chain family member 4 regulates axonal transport of synaptic vesicles and is required for synaptic development and transmission. J Neurosci 31:2052–2063. CrossRef Medline

Liu Z, Chen Y, Wang D, Wang S, Zhang YQ (2010) Distinct presynaptic and postsynaptic dismantling processes of *Drosophila* neuromuscular junctions during metamorphosis. J Neurosci 30:11624–11634. CrossRef Medline

Marie B, Sweeney ST, Poskanzer KE, Roos J, Kelly RB, Davis GW (2004) Dap160/intersectin scaffolds the periactive zone to achieve high-fidelity endocytosis and normal synaptic growth. Neuron 43:207–219. CrossRef Medline

Martin AR (1955) A further study of the statistic composition of the endplate potential. J Physiol 130:114–122. Medline

Menon KP, Sanyal S, Habara Y, Sanchez R, Wharton RP, Ramaswami M, Zinn K (2004) The translational repressor pumilio regulates presynaptic morphology and controls postsynaptic accumulation of translation factor elF-4E. Neuron 44:663–676. CrossRef Medline

Menon KP, Andrews S, Murthy M, Gavis ER, Zinn K (2009) The translational repressors Nanos and Pumilio have divergent effects on presynaptic terminal growth and postsynaptic glutamate receptor subunit composition. J Neurosci 29:5558–5572. CrossRef Medline

Mosca TJ, Hong W, Dani VS, Favaloro V, Luo L (2012) Trans-synaptic Teneurin signalling in neuromuscular synapse organization and target choice. Nature 484:237–241. CrossRef Medline

Muraro NI, Weston AJ, Gerber AP, Luschnig S, Moffat KG, Baines RA (2008) Pumilio binds *para* mRNA and requires Nanos and brat to regulate sodium current in *Drosophila* motoneurons. J Neurosci 28: 2099–2109. CrossRef Medline

Nahm M, Kim S, Paik SK, Lee M, Lee S, Lee ZH, Kim J, Lee D, Bae YC (2010a) dCIP4 (*Drosophila* Cdc42-interacting protein 4) restrains synaptic growth by inhibiting the secretion of the retrograde glass bottom boat signal. J Neurosci 30:8138–8150. CrossRef Medline

Nahm M, Long AA, Paik SK, Kim S, Bae YC, Broadie K, Lee S (2010b) The Cdc42-selective GAP rich regulates postsynaptic development and retrograde BMP transsynaptic signaling. J Cell Biol 191:661–675. CrossRef Medline

O'Connor-Giles KM, Ho LL, Ganetzky B (2008) Nervous wreck interacts with thickveins and the endocytic machinery to attenuate retrograde BMP signaling during synaptic growth. Neuron 58:507–518. CrossRef Medline

Olesnicky EC, Bhogal B, Gavis ER (2012) Combinatorial use of translational cofactors for cell type-specific regulation during neuronal morphogenesis in *Drosophila*. Dev Biol 365:208–218. CrossRef Medline

Persson U, Izumi H, Souchelnytskyi S, Itoh S, Grimsby S, Engström U, Heldin CH, Funa K, ten Dijke P (1998) The L45 loop in type I receptors for TGF-β family members is a critical determinant in specifying Smad isoform activation. FEBS Lett 434:83–87. CrossRef Medline

Pielage J, Fetter RD, Davis GW (2006) A postsynaptic spectrin scaffold defines active zone size, spacing, and efficacy at the *Drosophila* neuromuscular junction. J Cell Biol 175:491–503. CrossRef Medline

Qin G, Schwarz T, Kittel RJ, Schmid A, Rasse TM, Kappei D, Ponimaskin E, Heckmann M, Sigrist SJ (2005) Four different subunits are essential for expressing the synaptic glutamate receptor at neuromuscular junctions of *Drosophila*. J Neurosci 25:3209–3218. CrossRef Medline

Rodal AA, Motola-Barnes RN, Littleton JT (2008) Nervous wreck and Cdc42 cooperate to regulate endocytic actin assembly during synaptic growth. J Neurosci 28:8316–8325. CrossRef Medline

Schulte J, Sepp KJ, Jorquera RA, Wu C, Song Y, Hong P, Littleton JT (2010) DMob4/Phocein regulates synapse formation, axonal transport, and microtubule organization. J Neurosci 30:5189–5203. CrossRef Medline

Sonoda J, Wharton RP (2001) *Drosophila* brain tumor is a translational repressor. Genes Dev 15:762–773. CrossRef Medline

Stefanatos RK, Vidal M (2011) Tumor invasion and metastasis in *Drosophila*: a bold past, a bright future. J Genet Genomics 38:431–438. CrossRef Medline

Sweeney ST, Davis GW (2002) Unrestricted synaptic growth in *spinster*-a late endosomal protein implicated in TGF-beta-mediated synaptic growth regulation. Neuron 36:403–416. CrossRef Medline

Takaesu NT, Herbig E, Zhitomersky D, O'Connor MB, Newfeld SJ (2005) DNA-binding domain mutations in SMAD genes yield dominant-negative proteins or a neomorphic protein that can activate WG target genes in *Drosophila*. Development 132:4883–4894. CrossRef Medline

Verstreken P, Kjaerulff O, Lloyd TE, Atkinson R, Zhou Y, Meinertzhagen IA, Bellen HJ (2002) *Endophilin* mutations block clathrin-mediated endocytosis but not neurotransmitter release. Cell 109:101–112. CrossRef Medline

Verstreken P, Ohyama T, Bellen HJ (2008) FM 1–43 labeling of synaptic vesicle pools at the *Drosophila* neuromuscular junction. Methods Mol Biol 440:349–369. CrossRef Medline

Verstreken P, Ohyama T, Haueter C, Habets RL, Lin YQ, Swan LE, Ly CV, Venken KJ, De Camilli P, Bellen HJ (2009) Tweek, an evolutionarily conserved protein, is required for synaptic vesicle recycling. Neuron 63: 203–215. CrossRef Medline

Wang D, Zhang L, Zhao G, Wahlstrom G, Heino TI, Chen J, Zhang YQ (2010) *Drosophila* twinfilin is required for cell migration and synaptic endocytosis. J Cell Sci 123:1546–1556. CrossRef Medline

Wang X, Shaw WR, Tsang HT, Reid E, O'Kane CJ (2007) *Drosophila* spichthyin inhibits BMP signaling and regulates synaptic growth and axonal microtubules. Nat Neurosci 10:177–185. CrossRef Medline

Wucherpfennig T, Wilsch-Bräuninger M, González-Gaitan M (2003) Role of *Drosophila* Rab5 during endosomal trafficking at the synapse and evoked neurotransmitter release. J Cell Biol 161:609–624. CrossRef Medline

Yao A, Jin S, Li X, Liu Z, Ma X, Tang J, Zhang YQ (2011) *Drosophila* FMRP regulates microtubule network formation and axonal transport of mitochondria. Hum Mol Genet 20:51–63. CrossRef Medline

Yao CK, Lin YQ, Ly CV, Ohyama T, Haueter CM, Moiseenkova-Bell VY, Wensel TG, Bellen HJ (2009) A synaptic vesicle-associated Ca^{2+} channel promotes endocytosis and couples exocytosis to endocytosis. Cell 138:947–960. CrossRef Medline

Zhang B, Koh YH, Beckstead RB, Budnik V, Ganetzky B, Bellen HJ (1998) Synaptic vesicle size and number are regulated by a clathrin adaptor protein required for endocytosis. Neuron 21:1465–1475. CrossRef Medline

Zhao L, Wang D, Wang Q, Rodal AA, Zhang YQ (2013) *Drosophila cyfip* regulates synaptic development and endocytosis by suppressing filamentous actin assembly. PLoS Genet 9:e1003450. CrossRef Medline